

Extended scalar sectors at future colliders*

TANIA ROBENS

Theoretical Physics Division, Rudjer Boskovic Institute, 10002 Zagreb, Croatia

JAN KALINOWSKI, ALEKSANDER FILIP ŻARNECKI

Faculty of Physics, University of Warsaw, ul. Pasteura 5, 02–093 Warsaw, Poland

ANDREAS PAPAEFSTATHIOU

Department of Physics, Kennesaw State University, Kennesaw, GA 30144, USA

After the discovery of the Higgs boson in 2012, particle physics has entered an exciting era. An important question is whether the Standard Model of particle physics correctly describes the scalar sector realized by nature, or whether it is part of a more extended model, featuring additional particle content. A prime way to test this is to probe models with extended scalar sectors at future collider facilities. We here discuss such models in the context of high-luminosity LHC, a possible proton-proton collider with 27 and 100 TeV center-of-mass energy, as well as future lepton colliders with various center-of-mass energies.

PACS numbers: 12.60.Fr,12.60.-i,13.66.Hk,14.80.Ec,14.80.Fd
RBI-ThPhys-2021-14

1. Introduction

After the discovery of a scalar which complies with the properties of the Higgs boson h of the Standard Model (SM) [1, 2], particle physics has entered an exciting era. One important question is whether the particle discovered by the LHC experiments indeed corresponds to the Higgs boson predicted by the Standard Model, or whether it is part of a model featuring an extended scalar sector. So far, both theoretical as experimental uncertainties allow for both options, although in general the parameter space of new physics models becomes increasingly constrained by both direct searches as

* Presented by Tania Robens at XXVII Cracow EIPHANY Conference of Future of particle physics

well as indirect probes, as e.g. the 125 GeV scalar coupling strength or electroweak precision observables (see e.g. [3, 4] for recent results).

In this work, we will discuss the discovery prospects of models with extended scalar sectors at future collider facilities. We will concentrate on two different scenarios: (a) The Inert Doublet Model, a two-Higgs-doublet model that features an exact \mathbb{Z}_2 symmetry. This model introduces 5 additional particles in the so-called dark sector and provides a dark matter candidate. (b) The two-real singlet extension of the Standard Model, where the scalar sector is enhanced by two real scalar singlets. In this model, an exact $\mathbb{Z}_2 \otimes \mathbb{Z}'_2$ symmetry is assumed, which is successively broken by the vacuum expectation values (vevs) of the two additional scalar fields. This induces mixing between all CP-even scalar states. This model features a plethora of new physics channels which so far have not been investigated by the LHC experiments. We will briefly discuss these and subsequently focus on the discovery prospects for hhh production within this model at LHC Run III as well as High-Luminosity LHC.

The two models described above will be covered in the subsequent sections of this manuscript. Section 2 will discuss the Inert Doublet Model, current status as well as possible future collider prospects. In section 3, on the other hand, we will comment on the two-real-singlet extension, with a special focus on discovery prospects for the hhh final state at the HL-LHC. We will conclude in section 4.

2. The Inert Doublet Model

2.1. The model

The Inert Doublet Model (IDM) [5, 6, 7] is an intriguing new physics model that enhances the SM scalar sector by an additional $SU(2) \times U(1)$ gauge doublet ϕ_D . Furthermore, it introduces a discrete \mathbb{Z}_2 symmetry with the following transformation properties

$$\phi_S \rightarrow \phi_S, \phi_D \rightarrow -\phi_D, \text{SM} \rightarrow \text{SM}. \quad (1)$$

In this model the symmetry remains exact. This has important consequences: (a) the additional doublet does not acquire a vacuum expectation value (vev) and (b) it does not couple to fermions. Therefore, electroweak symmetry breaking proceeds as in the SM. Furthermore, the above symmetry insures that the lightest particle of the so-called dark doublet ϕ_D is stable and renders a dark matter candidate.

The potential of the model is given by

$$V = -\frac{1}{2} \left[m_{11}^2 (\phi_S^\dagger \phi_S) + m_{22}^2 (\phi_D^\dagger \phi_D) \right] + \frac{\lambda_1}{2} (\phi_S^\dagger \phi_S)^2 + \frac{\lambda_2}{2} (\phi_D^\dagger \phi_D)^2 + \lambda_3 (\phi_S^\dagger \phi_S) (\phi_D^\dagger \phi_D) + \lambda_4 (\phi_S^\dagger \phi_D) (\phi_D^\dagger \phi_S) + \frac{\lambda_5}{2} \left[(\phi_S^\dagger \phi_D)^2 + (\phi_D^\dagger \phi_S)^2 \right]. \quad (2)$$

After electroweak symmetry breaking, the model features 7 free parameters. We here chose these in the so-called physical basis [8]

$$v, M_h, M_H, M_A, M_{H^\pm}, \lambda_2, \lambda_{345}, \quad (3)$$

where we use $\lambda_{345} \equiv \lambda_3 + \lambda_4 + \lambda_5$ throughout this work. The vev v as well as $M_h \sim 125$ GeV are fixed by experimental measurements, leading to a total number of 5 free parameters. We here choose H as the dark matter candidate, which implies $M_{A, H^\pm} \geq M_H$.¹

The model is subject to a large number of theoretical and experimental constraints. These have been discussed at length e.g. in [8, 9, 10, 11, 12] and will therefore not be repeated here. In the scan for the allowed parameter ranges, we make use of the publicly available tools 2HDMC [13], HiggsBounds-5.9.0 [14, 15, 16, 17, 18], HiggsSignals-2.6.0 [19, 20], as well as micrOMEGAs_5.2.4 [21]. Cross sections are calculated using Madgraph5 [22] with a UFO input file from [23]². We compare to experimental values from GFitter [26, 27], as well as results from the Planck [28] and XENON1T [29] experiments. Direct collider searches as well as agreement with the 125 GeV coupling strength measurements are implemented via HiggsBounds and HiggsSignals, where we additionally compare to the total width upper limit [30] and invisible branching ratio [31] of h . Recast results from a LEP-SUSY search [32] were also included. We refer the reader to the above references for more details.

2.2. Current Status

The experimental and theoretical constraints lead to a large reduction of the allowed parameter space of the model; in particular, the masses are usually constrained to be quite degenerate, as can be seen from figure 1. This is due to an interplay of electroweak constraints as well as theoretical requirements on the potential. A particularly interesting scenario is the case when $M_H \leq M_h/2$, which opens up the $h \rightarrow$ invisible channel. In such a scenario, there is an interesting interplay between bounds from signal strength measurements, that require $|\lambda_{345}|$ to be rather small $\lesssim 0.3$, and bounds from dark matter relic density, where too low values of that parameter lead to small annihilation cross sections and therefore too large

¹ Note that the new scalars in the IDM do not have CP quantum numbers, as they do not couple to fermions. In the subsequent discussion, we can replace $H \longleftrightarrow A$ if we simultaneously use $\lambda_5 \longleftrightarrow -\lambda_5$. All phenomenological considerations are identical for these cases.

² Note the official version available at [24] exhibits a wrong CKM structure, leading to false results for processes involving electroweak gauge bosons radiated off quark lines. In our implementation, we corrected for this. Our implementation corresponds to the expressions available from [25].

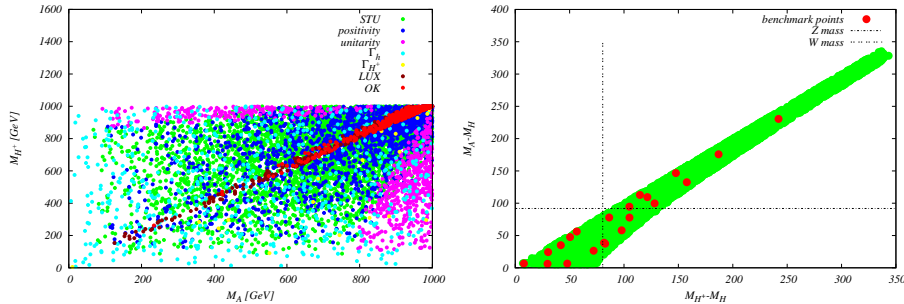


Fig. 1. Masses are requested to be quite degenerate after all constraints have been taken into account. *Left*: In the (M_A, M_{H^\pm}) plane (taken from [8]). *Right*: In the $(M_{H^\pm} - M_H, M_A - M_H)$ plane (taken from [11]).

relic density values. The effects of this are shown in figure 2. In [8], it was found that this in general leads to a lower bound of $M_H \sim 50$ GeV, although exceptions to this rule were presented in [12].

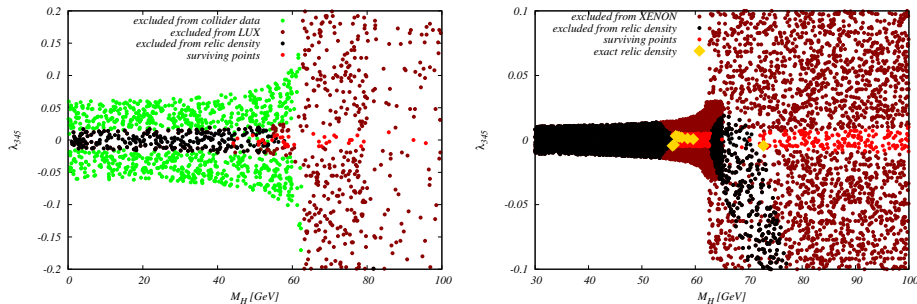


Fig. 2. Interplay of signal strength and relic density constraints in the (M_H, λ_{345}) plane. *Left*: Using LUX constraints [33], bounds labelled "excluded from collider data" have been tested using `HiggsBounds` and `HiggsSignals` (taken from [8]). *Right*: Using XENON1T results, with golden points labelling those points that produce exact relic density (taken from [9]).

2.3. Discovery prospects at CLIC

So far, no publicly available search exists that investigates the IDM parameter space with actual collider data. In [34, 35], however, the discovery potential of CLIC was investigated for several benchmark points proposed in [11], for varying center-of-mass energies up to 3 TeV. We investigated both AH and H^+H^- production with $A \rightarrow ZH$ and $H^\pm \rightarrow W^\pm H$, where the

electroweak gauge bosons subsequently decay leptonically. Event generation was performed using `WHizard 2.2.8` [36, 37], with an interface via `SARAH` [38] and `SPheno 4.0.3` [39, 40] for model implementation. CLIC energy spectra [41] were also taken into account.

For the production modes above, we considered leptonic decays of the electroweak gauge bosons. In particular, the investigated final states were

$$e^+ e^- \rightarrow \mu^+ \mu^- + \cancel{E}, e^+ e^- \rightarrow \mu^\pm e^\mp + \cancel{E}$$

for HA and $H^+ H^-$ production, respectively. Note however, that in the event generation we did not specify the intermediate states, which means all processes leading to the above signatures were taken into account, including interference between the contributing diagrams. This includes final states where the missing energy can originate from neutrinos in the final state.

Event selection was performed using a set of preselection cuts as well as boosted decision trees, as implemented in the TMVA toolkit [42]. Results for the discovery reach of CLIC with varying center of mass energies are shown in figure 3. We see that in general, production cross sections $\gtrsim 0.5$ fb seem to be accessible, where best prospects for the considered benchmark points are given for 380 GeV or 1.5 TeV center-of-mass energies. Similarly, mass sums up to 1 TeV seem accessible, where in general the $\mu^\pm e^\mp$ channel seems to provide a larger discovery range. Considering the $H^+ H^-$ production with the semi-leptonic final state, i.e. with hadronic decay of one of the W bosons, increases the corresponding mass range to about 2 TeV [43, 44, 45, 46].

2.4. Sensitivity comparison at future colliders

After a dedicated analysis of the IDM benchmarks in the CLIC environment, an important question is whether other current or future collider options provide similar or better discovery prospects. Therefore, for the benchmarks proposed in [11, 34], production cross sections for a variety of processes have been presented in [12], including VBF-type topologies. Cross sections were calculated using `Madgraph5`. We list the considered collider types and nominal center-of-mass energies as well as integrated luminosities in table 1.

We here label a scenario "realistic" when we can expect 1000 events to be produced using target luminosity and center-of-mass energies as specified above. Obviously, more detailed studies, including both background contribution and detector response simulation, are necessary to assess the actual collider reach.

We consider the following production modes:

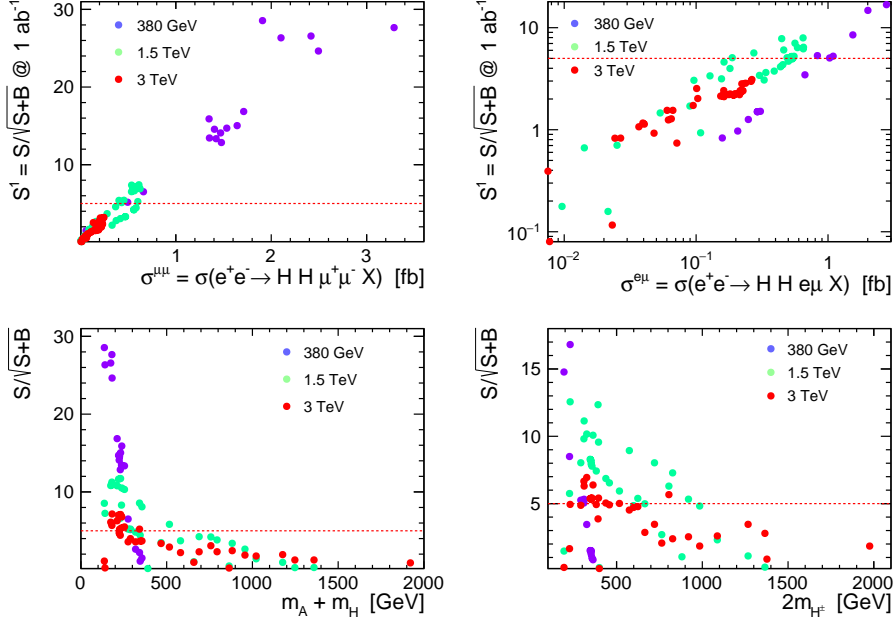


Fig. 3. Discovery prospects at CLIC for the IDM in $\mu^+\mu^- + \cancel{E}$ (left) and $\mu^\pm e^\mp + \cancel{E}$ (right) final states, as a function of the respective production cross-sections (top) and mass sum of the produced particles (bottom). Taken from [34].

collider	cm energy [TeV]	$\int \mathcal{L}$	σ_{1000} [fb]
HL-LHC	13/ 14	3 ab^{-1}	0.33
HE-LHC	27	15 ab^{-1}	0.07
FCC-hh	100	20 ab^{-1}	0.05
ee	3	5 ab^{-1}	0.2
$\mu\mu$	10	10 ab^{-1}	0.1
$\mu\mu$	30	90 ab^{-1}	0.01

Table 1. Collider parameters used in the discovery reach study performed in [12]. Collider specifications have been taken from [47, 48, 49, 50, 51] for the HL-LHC, HE-LHC, FCC-hh and muon collider, respectively. The last column denotes the minimal cross section required to produce 1000 events using full target luminosity.

- **pp colliders at various center-of-mass energies:**

$$pp \rightarrow HA, HH^+, HH^-, AH^+, AH^-, H^+H^-, AA,$$

$$pp \rightarrow AAjj, H^+H^-jj.$$

The latter two processes are labelled "VBF-like" topologies, although in practise we include all diagrams that contribute to that specific final state; e.g., to the $AAjj$ final state, also $H^\pm A$ production contributes, with subsequent decays $H^\pm \rightarrow W^\pm A$ and hadronic decays of the W . Furthermore, all but the AA direct pair production are proportional to couplings from the SM electroweak sector (see e.g. [8]), so in principle these production cross sections are determined by the masses of the pair-produced particles. The AA channel is proportional to

$$\bar{\lambda}_{345} = \lambda_{345} - 2 \frac{M_H^2 - M_A^2}{v^2}, \quad (4)$$

so dependences here are more involved.

- **$\mu\mu$ colliders:**

At the muon collider, we mainly consider

$$\mu^+ \mu^- \rightarrow \nu_\mu \bar{\nu}_\mu AA, \quad \mu^+ \mu^- \rightarrow \nu_\mu \bar{\nu}_\mu H^+ H^-.$$

which again corresponds to VBF-like production modes. However, as before, we do not specify intermediate states, so in fact several diagrams contribute which not all have a typical VBF topology. See appendix B and C of [12] for details.

Figures 4 and 5 show the production cross sections as a function of the mass sum of produced particles for various collider options and production modes. We see clearly that, while predictions for direct pair-production cross sections at pp colliders exhibit a fall with rising mass-scales for all but the AA pair-production mode, understanding the behaviour of the VBF-induced channels is less trivial. This can be attributed to the fact that more diagrams contribute. For example, for $AAjj$ we have contributions from h - exchange in the s-channel which are again proportional to $\bar{\lambda}_{345}$ given by eqn. (4), which can induce large jumps between cross-section predictions for scenarios with similar mass scales. Similar differences can be observed for VBF-type production at $\mu\mu$ colliders; this can be traced back mainly to a fine-tuned cancellation of various contributing diagrams, which is discussed in large detail in [12].

The summary of sensitivities in terms of mass scales is given in table 2.

We see that especially for AA production the VBF mode at both proton and muon colliders serves to significantly increase the discovery reach of the respective machine. Using the simple counting criterium above, we can furthermore state that a 27 TeV proton-proton machine has a similar reach

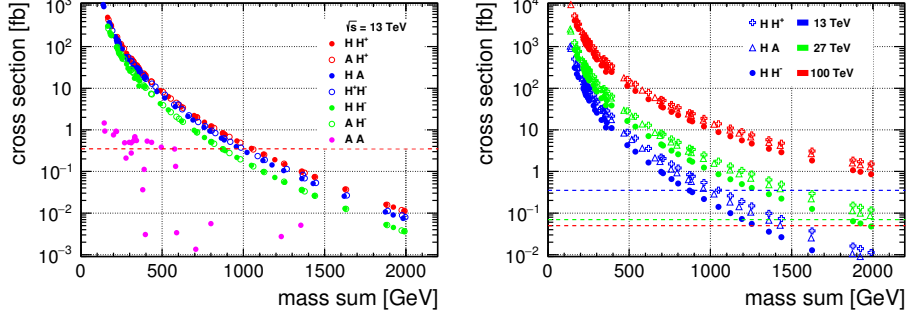


Fig. 4. Pair-production cross-section predictions at pp colliders as a function of the sum of produced particle masses. *Left*: For all considered production channels at 13 TeV LHC. *Right*: for selected channels at 13 TeV, 27 TeV, and 100 TeV. Horizontal dashed lines denote the limit of the cross section at which 1000 events are produced with the respective target luminosity, cf table 1. Taken from [12].

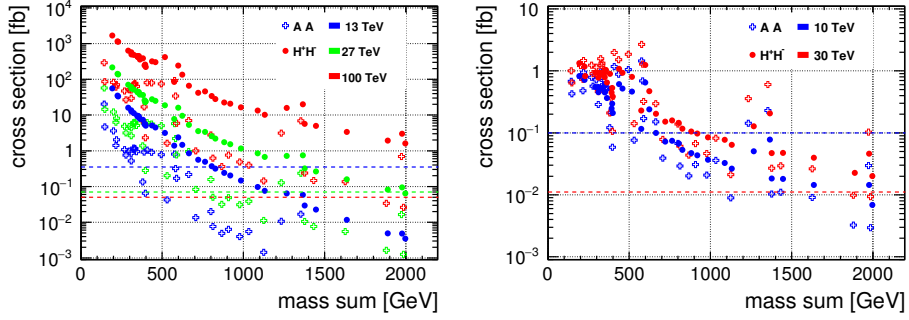


Fig. 5. As figure 4, but now considering the VBF-type production mode. *Left*: for pp colliders, where two additional jets are produced and *right*: at $\mu\mu$ colliders. Taken from [12].

as a 10 TeV muon collider, while 100 TeV FCC-hh would correspond to a 30 TeV muon-muon machine. Obviously, detailed investigations including SM background are needed to give a more realistic estimate of the respective collider reach.

collider	all others	AA	AA +VBF
HL-LHC	1 TeV	200-600 GeV	500-600 GeV
HE-LHC	2 TeV	400-1400 GeV	800-1400 GeV
FCC-hh	2 TeV	600-2000 GeV	1600-2000 GeV
CLIC, 3 TeV	2 TeV	-	300-600 GeV
$\mu\mu$, 10 TeV	2 TeV	-	400-1400 GeV
$\mu\mu$, 30 TeV	2 TeV	-	1800-2000 GeV

Table 2. Sensitivity of different collider options specified in table 1, using the sensitivity criterium of 1000 generated events in the specific channel. $x - y$ denotes minimal/ maximal mass scales that are reachable. Numbers for CLIC correspond to results from detailed investigations [34, 35].

3. Two-real-singlet extension

3.1. The model

The two-real-singlet model (TRSM) is a model that features the extension of the SM scalar sector by two additional real singlets S, X , which obey a $\mathbb{Z}_2 \otimes \mathbb{Z}_2$ symmetry. It has been introduced in [52], with a first phenomenological study of the model being presented in [53]. The model is also available in the public tool **ScannerS** [54, 55, 56].

The transformation properties under the two discrete symmetries are specified as

$$\begin{aligned} \mathbb{Z}_2^S : S &\rightarrow -S, X \rightarrow X, \text{ SM} \rightarrow \text{SM}, \\ \mathbb{Z}_2^X : X &\rightarrow -X, S \rightarrow S, \text{ SM} \rightarrow \text{SM}. \end{aligned} \quad (5)$$

Application of this symmetry reduces the number of possible terms in the potential, such that we obtain

$$\begin{aligned} V = \mu_\Phi^2 \Phi^\dagger \Phi + \lambda_\Phi (\Phi^\dagger \Phi)^2 + \mu_S^2 S^2 + \lambda_S S^4 + \mu_X^2 X^2 + \lambda_X X^4 \\ + \lambda_{\Phi S} \Phi^\dagger \Phi S^2 + \lambda_{\Phi X} \Phi^\dagger \Phi X^2 + \lambda_{SX} S^2 X^2. \end{aligned} \quad (6)$$

So far, we have not specified whether the additional scalar states acquire vevs. In fact, setting one of these to zero opens up the possibility of having a portal-like dark matter scenario. On the other hand, when both additional fields acquire a vev, the above symmetry is softly broken and all scalar fields mix. We here discuss this second scenario. The gauge-eigenstates are then given by

$$\Phi = \begin{pmatrix} 0 \\ \frac{\phi_h + v}{\sqrt{2}} \end{pmatrix}, \quad S = \frac{\phi_S + v_S}{\sqrt{2}}, \quad X = \frac{\phi_X + v_X}{\sqrt{2}} \quad (7)$$

Rotation into mass eigenstates is then described by a rotation matrix R , with

$$\begin{pmatrix} h_1 \\ h_2 \\ h_3 \end{pmatrix} = R \begin{pmatrix} \phi_h \\ \phi_S \\ \phi_X \end{pmatrix}. \quad (8)$$

where in the following we adapt the convention that

$$M_1 \leq M_2 \leq M_3.$$

The rotation matrix is described via three mixing angles $\theta_{1,2,3}$, with

$$R = \begin{pmatrix} c_1 c_2 & -s_1 c_2 & -s_2 \\ s_1 c_3 - c_1 s_2 s_3 & c_1 c_3 + s_1 s_2 s_3 & -c_2 s_3 \\ c_1 s_2 c_3 + s_1 s_3 & c_1 s_3 - s_1 s_2 c_3 & c_2 c_3 \end{pmatrix}. \quad (9)$$

with the short-hand notation

$$s_1 \equiv \sin \theta_{hS}, \quad s_2 \equiv \sin \theta_{hX}, \quad s_3 \equiv \sin \theta_{SX}, \quad c_1 \equiv \cos \theta_{hS}, \dots \quad (10)$$

It is important to note that all interactions to SM particles are inherited through this mixing, with a corresponding scaling factor $\kappa_i \equiv R_{i1}$ for the mass eigenstate h_i .

After electroweak symmetry breaking, the model has in total 9 free parameters; as before, two of these, $v \simeq 246$ GeV and $M_a \simeq 125$ GeV, are fixed by the Higgs mass measurement and electroweak precision observables. We then choose as free input parameters

$$M_b, M_c, \theta_{hS}, \theta_{hX}, \theta_{SX}, v_S, v_X, \quad (11)$$

with $a \neq b \neq c \in \{1, 2, 3\}$.

As before, the model is subject to a large number of theoretical and experimental constraints, which have been presented in detail in [52] and will not be repeated here.

3.2. Phenomenology and benchmark planes

Having three distinct scalar final states, this model allows for interesting scalar-scalar production and decay modes. At pp colliders, we have

$$\begin{aligned} pp &\rightarrow h_3 \rightarrow h_1 h_1; & pp &\rightarrow h_3 \rightarrow h_2 h_2; \\ pp &\rightarrow h_2 \rightarrow h_1 h_1; & pp &\rightarrow h_3 \rightarrow h_1 h_2 \end{aligned}$$

with decay modes given by

benchmark scenario	h_{125}	target signature	possible successive decays
BP1	h_3	$h_{125} \rightarrow h_1 h_2$	$h_2 \rightarrow h_1 h_1$ if $M_2 > 2M_1$
BP2	h_2	$h_3 \rightarrow h_1 h_{125}$	-
BP3	h_1	$h_3 \rightarrow h_{125} h_2$	$h_2 \rightarrow h_{125} h_{125}$ if $M_2 > 250$ GeV
BP4	h_3	$h_2 \rightarrow h_1 h_1$	-
BP5	h_2	$h_3 \rightarrow h_1 h_1$	-
BP6	h_1	$h_3 \rightarrow h_2 h_2$	$h_2 \rightarrow h_{125} h_{125}$ if $M_2 > 250$ GeV

Table 3. Overview of the benchmark scenarios: The second column denotes the Higgs mass eigenstate that we identify with the observed Higgs boson, h_{125} , the third column names the targeted decay mode of the resonantly produced Higgs state, and the fourth column lists possible relevant successive decays of the resulting Higgs states. Taken from [52].

$$h_2 \rightarrow \text{SM}; h_2 \rightarrow h_1 h_1; h_1 \rightarrow \text{SM}$$

The exact phenomenology depends on the chosen parameter point. While all partial decay widths to SM-like final states are given by the common scaling factors defined above

$$\Gamma(h_a \rightarrow \text{SM}; M_a) = \kappa_a^2 \cdot \Gamma_{\text{tot}}(h_{\text{SM}}; M_a), \quad (12)$$

where $\Gamma_{\text{tot}}(h_{\text{SM}}; M_a)$ denotes the decay width of a SM-like scalar of mass M_a , partial decays into scalar final states need to be calculated from the new physics parameters in the potential.

In [52], a number of benchmark planes was defined in order to accommodate for production and decay modes in the scalar sector that are currently not investigated by the LHC experiments. We list these in table 3.

For some of these, especially BP4, BP5, and BP1, relatively high production rates of 60 pb, 2.5 pb, and 3 pb respectively can be achieved at the 13 TeV LHC. These numbers correspond to rescaled production modes

$$\sigma(M_a) = \kappa_a^2 \cdot \sigma_{\text{SM}}(M_a). \quad (13)$$

followed by factorized decays. $\sigma_{\text{SM}}(M_a)$ denotes the NNLO+NNLL production cross section for a SM-like Higgs of mass M_a , with numbers taken from [57]. The relatively large rates make these BPs prime targets for current LHC data analyses. In the following, we however concentrate on BP3 and the hhh final state.

Parameter	Value
M_1	125.09 GeV
M_2	[125, 500] GeV
M_3	[255, 650] GeV
θ_{hS}	-0.129
θ_{hX}	0.226
θ_{SX}	-0.899
v_S	140 GeV
v_X	100 GeV
κ_1	0.966
κ_2	0.094
κ_3	0.239

Table 4. The numerical values for the independent parameter values of eq. (11) that characterise **BP3**. The Higgs doublet vev, v , is fixed to 246 GeV. The κ_i values correspond to the rescaling parameters of the SM-like couplings for the respective scalars and are derived quantities.

3.3. hhh production in the TRSM

One interesting scenario within the TRSM is the asymmetric production and subsequent decay

$$pp \rightarrow h_3 \rightarrow h_2 h_1 \rightarrow h_1 h_1 h_1, \quad (14)$$

where $h_1 \equiv h$ is the SM-like scalar. This signature is realized in BP3 and was analysed in detail in [53]. Input parameters for BP3 are displayed in table 4.

We want to briefly comment on the calculation of rates, and differences between these in [52] and [53]:

- In [52], production cross sections were calculated as specified in eqn. (13), and rates for final states were then derived via multiplication with the corresponding branching ratios. This is a priori a good approach for a first estimate, and incorporates important higher-order effects in the production cross sections.
- In [53], on the other hand, we made use of a customized `loop_sm` model implemented in `MadGraph5_aMC@NLO` (v2.7.3) [58, 59], and subsequently interfaced to `HERWIG` (v7.2.1) [60, 61, 62, 63, 64, 65, 66]. This model includes full top and bottom mass effects and calculates production modes at LO, i.e. at the one-loop level. Furthermore, for

the process (14) intermediate states were not specified, which guarantees the inclusion of all contributing diagrams as well as interference effects. In particular, in some scenarios contributions from s -channel offshell h_1 states were on the % level.

Taking this into account, we display in figure 6 the production cross section for the hh_2 final state as derived in [52]. For this final state, production cross sections can reach up to 0.3 pb. Branching ratios for h_2 and hh_2 are

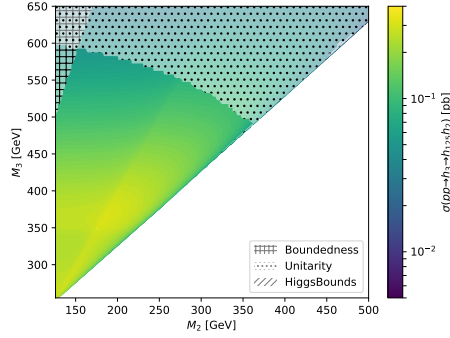


Fig. 6. Production cross section for the hh_2 final state in BP3 at a 13 TeV LHC, as a function of M_2 and M_3 . Experimental exclusion bounds stem from searches for $h_{2,3} \rightarrow VV$ from 2016 LHC Run II data [67, 68, 69]. Taken from [52].

displayed in figure 7. This particular benchmark plane was chosen such that

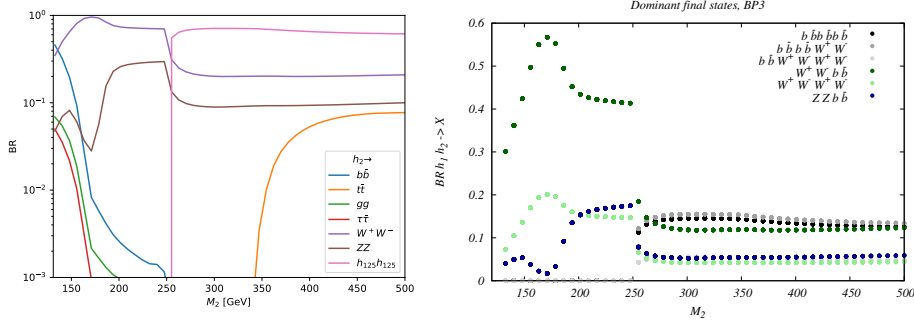


Fig. 7. Branching ratios for h_2 (left) and hh_2 (right) in BP3, as a function of M_2 . Left plot taken from [52].

$h_2 \rightarrow hh$ becomes dominant as soon as it is kinematically allowed. This induces the predominance of $b\bar{b}b\bar{b}b\bar{b}$ and $b\bar{b}b\bar{b}W^+W^-$ rates over those for four-particle final states.

(M_2, M_3) [GeV]	$\sigma(pp \rightarrow h_1 h_1 h_1)$ [fb]	$\sigma(pp \rightarrow 3b\bar{b})$ [fb]	sig $_{300\text{fb}^{-1}}$	sig $_{3000\text{fb}^{-1}}$
(255, 504)	32.40	6.40	2.92	9.23
(263, 455)	50.36	9.95	4.78	15.10
(287, 502)	39.61	7.82	4.01	12.68
(290, 454)	49.00	9.68	5.02	15.86
(320, 503)	35.88	7.09	3.76	11.88
(264, 504)	37.67	7.44	3.56	11.27
(280, 455)	51.00	10.07	5.18	16.39
(300, 475)	43.92	8.68	4.64	14.68
(310, 500)	37.90	7.49	4.09	12.94
(280, 500)	40.26	7.95	4.00	12.65

Table 5. Benchmark points investigated in [53], leading-order production cross sections at 14 TeV, as well as significances for different integrated luminosities.

In [53], several benchmark points were selected which were then investigated at the LHC using 14 TeV center-of-mass energy, where we concentrated in the $b\bar{b}b\bar{b}$ final state. Those benchmark points as well as significances for an integrated luminosity of $\int \mathcal{L} = 300 \text{ fb}^{-1}$ and $\int \mathcal{L} = 3000 \text{ fb}^{-1}$ are shown in table 5.

For details of the analysis as well as SM background simulation, we refer the reader to the above work. We see that several of the benchmark points are in the 4-5 σ range already for a relatively low luminosity, and all have significances above the discovery reach after the full run of HL-LHC. We therefore strongly encourage the experimental collaborations to adapt our search strategy, using actual LHC data.

Finally, we can ask whether other channels can not equally constrain the allowed parameter space at the HL-LHC. To this end, we have extrapolated various analyses assessing the heavy Higgs boson prospects of the HL-LHC in final states originating from $h_i \rightarrow h_1 h_1$ [70, 71], $h_i \rightarrow ZZ$ [68, 72] and $h_i \rightarrow W^+ W^-$ [73, 74], for $i = 2, 3$, and combined these with extrapolations of results from 13 TeV where appropriate. Details of the extrapolation procedure can be found in Appendix D of ref. [75]. The corresponding results are shown in figure 8.

Especially ZZ final states can probe nearly all of the available parameter space. However, we want to emphasize that these depend on different model parameters than the $h_1 h_1 h_1$ final state rates, and therefore these searches can be considered as complementary, testing various parts of the new physics potential. We encourage the LHC experimental collaborations to pursue searches in all possible decay channels.

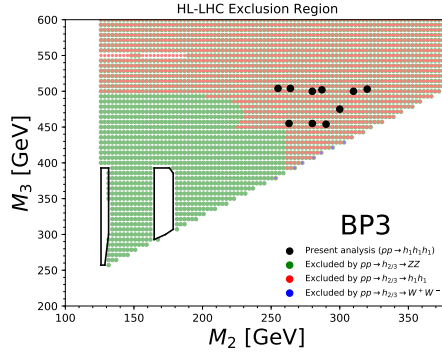


Fig. 8. Constraints on the (M_2, M_3) plane from extrapolation of other searches at the HL-LHC from extrapolation (see text for details). Taken from [53].

4. Conclusion

In this work, we have discussed several new physics models and their discovery prospects at future colliders. For the Inert Doublet Model, a two-Higgs doublet model with a dark matter candidate, we have discussed constraints on the parameter space and presented results of a dedicated study of several benchmark points in di-scalar production within the CLIC environment for several center-of-mass energies. We found that, when using both leptonic and semi-leptonic decay modes for these searches, mass scales up to 1 TeV could in principle be reachable. Furthermore, we have performed a simplified study where we compared collider reaches for IDM benchmark points using a simple counting criterium. We found that, especially for the elusive AA production channel, the inclusion of VBF-type production modes greatly enhances the mass range that could in principle be tested at colliders. This comparison should be taken as a starting point for more dedicated studies at both hadron-hadron and lepton-lepton machines.

Furthermore, we reported on the sensitivity of the HL-LHC for new physics-initiated cascade decays leading to hhh final states, with subsequent decays into $3 b\bar{b}$ pairs. We found that at the HL-LHC all considered benchmark points such be within discovery range, while some statements could already be made for several benchmark points for an integrated luminosity of a few hundred fb^{-1} . We strongly encourage the LHC experimental collaborations to adapt this search using current and future LHC data.

Acknowledgements

This research was supported in parts by the National Science Centre, Poland, the HARMONIA project under contract UMO-2015/18/M/ST2/00518 and OPUS project under contract UMO-2017/25/B/ST2/00496 (2018-2021), and by the European Union through the Programme Horizon 2020 via the COST actions CA15108 - FUNDAMENTALCONNECTIONS and CA16201 - PARTICLEFACE. Research discussed here was also supported by the UK's Royal Society.

REFERENCES

- [1] Georges Aad et al. Observation of a new particle in the search for the Standard Model Higgs boson with the ATLAS detector at the LHC. *Phys. Lett.*, B716:1–29, 2012, 1207.7214.
- [2] Serguei Chatrchyan et al. Observation of a New Boson at a Mass of 125 GeV with the CMS Experiment at the LHC. *Phys. Lett.*, B716:30–61, 2012, 1207.7235.
- [3] <https://twiki.cern.ch/twiki/bin/view/AtlasPublic/HiggsPublicResults>.
- [4] <http://cms-results.web.cern.ch/cms-results/public-results/publications/HIG/index.html>.
- [5] Nilendra G. Deshpande and Ernest Ma. Pattern of Symmetry Breaking with Two Higgs Doublets. *Phys. Rev.*, D18:2574, 1978.
- [6] Qing-Hong Cao, Ernest Ma, and G. Rajasekaran. Observing the Dark Scalar Doublet and its Impact on the Standard-Model Higgs Boson at Colliders. *Phys. Rev.*, D76:095011, 2007, 0708.2939.
- [7] Riccardo Barbieri, Lawrence J. Hall, and Vyacheslav S. Rychkov. Improved naturalness with a heavy Higgs: An Alternative road to LHC physics. *Phys. Rev.*, D74:015007, 2006, hep-ph/0603188.
- [8] Agnieszka Ilnicka, Maria Krawczyk, and Tania Robens. Inert Doublet Model in light of LHC Run I and astrophysical data. *Phys. Rev.*, D93(5):055026, 2016, 1508.01671.
- [9] Agnieszka Ilnicka, Tania Robens, and Tim Stefaniak. Constraining Extended Scalar Sectors at the LHC and beyond. *Mod. Phys. Lett.*, A33(10n11):1830007, 2018, 1803.03594.
- [10] Daniel Dercks and Tania Robens. Constraining the Inert Doublet Model using Vector Boson Fusion. *Eur. Phys. J.*, C79(11):924, 2019, 1812.07913.
- [11] Jan Kalinowski, Wojciech Kotlarski, Tania Robens, Dorota Sokolowska, and Aleksander Filip Zarnecki. Benchmarking the Inert Doublet Model for e^+e^- colliders. *JHEP*, 12:081, 2018, 1809.07712.
- [12] Jan Kalinowski, Tania Robens, Dorota Sokolowska, and Aleksander Filip Zarnecki. IDM benchmarks for the LHC and future colliders. 2020, 2012.14818.

- [13] David Eriksson, Johan Rathsmann, and Oscar Stål. 2HDMC: Two-Higgs-Doublet Model Calculator Physics and Manual. *Comput. Phys. Commun.*, 181:189–205, 2010, 0902.0851.
- [14] Philip Bechtle, Oliver Brein, Sven Heinemeyer, Georg Weiglein, and Karina E. Williams. HiggsBounds: Confronting Arbitrary Higgs Sectors with Exclusion Bounds from LEP and the Tevatron. *Comput. Phys. Commun.*, 181:138–167, 2010, 0811.4169.
- [15] Philip Bechtle, Oliver Brein, Sven Heinemeyer, Georg Weiglein, and Karina E. Williams. HiggsBounds 2.0.0: Confronting Neutral and Charged Higgs Sector Predictions with Exclusion Bounds from LEP and the Tevatron. *Comput. Phys. Commun.*, 182:2605–2631, 2011, 1102.1898.
- [16] Philip Bechtle, Oliver Brein, Sven Heinemeyer, Oscar Stål, Tim Stefaniak, Georg Weiglein, and Karina E. Williams. HiggsBounds – 4: Improved Tests of Extended Higgs Sectors against Exclusion Bounds from LEP, the Tevatron and the LHC. *Eur. Phys. J.*, C74(3):2693, 2014, 1311.0055.
- [17] Philip Bechtle, Sven Heinemeyer, Oscar Stål, Tim Stefaniak, and Georg Weiglein. Applying Exclusion Likelihoods from LHC Searches to Extended Higgs Sectors. *Eur. Phys. J.*, C75(9):421, 2015, 1507.06706.
- [18] Philip Bechtle, Daniel Dercks, Sven Heinemeyer, Tobias Klingl, Tim Stefaniak, Georg Weiglein, and Jonas Wittbrodt. HiggsBounds-5: Testing Higgs Sectors in the LHC 13 TeV Era. *Eur. Phys. J.*, C80(12):1211, 2020, 2006.06007.
- [19] Philip Bechtle, Sven Heinemeyer, Oscar Stal, Tim Stefaniak, and Georg Weiglein. *HiggsSignals*: Confronting arbitrary Higgs sectors with measurements at the Tevatron and the LHC. *Eur. Phys. J.*, C74(2):2711, 2014, 1305.1933.
- [20] Philip Bechtle, Sven Heinemeyer, Tobias Klingl, Tim Stefaniak, Georg Weiglein, and Jonas Wittbrodt. HiggsSignals-2: Probing new physics with precision Higgs measurements in the LHC 13 TeV era. *Eur. Phys. J.*, C81(2):145, 2021, 2012.09197.
- [21] Genevieve Belanger, Ali Mjallal, and Alexander Pukhov. Recasting direct detection limits within micrOMEGAs and implication for non-standard Dark Matter scenarios. *Eur. Phys. J.*, C81(3):239, 2021, 2003.08621.
- [22] Johan Alwall, Michel Herquet, Fabio Maltoni, Olivier Mattelaer, and Tim Stelzer. MadGraph 5 : Going Beyond. *JHEP*, 06:128, 2011, 1106.0522.
- [23] A. Goudelis, B. Herrmann, and O. Stal. Dark matter in the Inert Doublet Model after the discovery of a Higgs-like boson at the LHC. *JHEP*, 09:106, 2013, 1303.3010.
- [24] <https://feynrules.irmp.ucl.ac.be/wiki/ModelDatabaseMainPage>. (as checked on Dec. 18,2020).
- [25] P. A. Zyla et al. Review of Particle Physics. *PTEP*, 2020(8):083C01, 2020.
- [26] <http://project-gfitter.web.cern.ch/project-gfitter/>.
- [27] Johannes Haller, Andreas Hoecker, Roman Kogler, Klaus Moenig, Thomas Peiffer, and Joerg Stelzer. Update of the global electroweak fit and constraints on two-Higgs-doublet models. *Eur. Phys. J.*, C78(8):675, 2018, 1803.01853.

- [28] N. Aghanim et al. Planck 2018 results. VI. Cosmological parameters. *Astron. Astrophys.*, 641:A6, 2020, 1807.06209.
- [29] E. Aprile et al. Dark Matter Search Results from a One Tonne \times Year Exposure of XENON1T. *Phys. Rev. Lett.*, 121(11):111302, 2018, 1805.12562.
- [30] Albert M Sirunyan et al. Measurements of the Higgs boson width and anomalous HVV couplings from on-shell and off-shell production in the four-lepton final state. *Phys. Rev. D*, 99(11):112003, 2019, 1901.00174.
- [31] Combination of searches for invisible Higgs boson decays with the ATLAS experiment. Technical Report ATLAS-CONF-2020-052, CERN, Geneva, Oct 2020.
- [32] Erik Lundstrom, Michael Gustafsson, and Joakim Edsjo. The Inert Doublet Model and LEP II Limits. *Phys. Rev.*, D79:035013, 2009, 0810.3924.
- [33] D. S. Akerib et al. First results from the LUX dark matter experiment at the Sanford Underground Research Facility. *Phys. Rev. Lett.*, 112:091303, 2014, 1310.8214.
- [34] Jan Kalinowski, Wojciech Kotlarski, Tania Robens, Dorota Sokolowska, and Aleksander Filip Zarnecki. Exploring Inert Scalars at CLIC. *JHEP*, 07:053, 2019, 1811.06952.
- [35] R. Franceschini et al. The CLIC Potential for New Physics. 2018, 1812.02093.
- [36] Mauro Moretti, Thorsten Ohl, and Jurgen Reuter. O'Mega: An Optimizing matrix element generator. pages 1981–2009, 2001, hep-ph/0102195.
- [37] Wolfgang Kilian, Thorsten Ohl, and Jurgen Reuter. WHIZARD: Simulating Multi-Particle Processes at LHC and ILC. *Eur. Phys. J.*, C71:1742, 2011, 0708.4233.
- [38] Florian Staub. Exploring new models in all detail with SARAH. *Adv. High Energy Phys.*, 2015:840780, 2015, 1503.04200.
- [39] Werner Porod. SPheno, a program for calculating supersymmetric spectra, SUSY particle decays and SUSY particle production at e^+e^- colliders. *Comput. Phys. Commun.*, 153:275–315, 2003, hep-ph/0301101.
- [40] W. Porod and F. Staub. SPheno 3.1: Extensions including flavour, CP-phases and models beyond the MSSM. *Comput. Phys. Commun.*, 183:2458–2469, 2012, 1104.1573.
- [41] Lucie Linssen, Akiya Miyamoto, Marcel Stanitzki, and Harry Weerts. Physics and Detectors at CLIC: CLIC Conceptual Design Report. 2012, 1202.5940.
- [42] Andreas Hocker et al. TMVA - Toolkit for Multivariate Data Analysis. 2007, physics/0703039.
- [43] Dorota Sokolowska, Jan Kalinowski, Jan Klamka, Pawel Sopicki, Aleksander Filip Zarnecki, Wojciech Kotlarski, and Tania Robens. Inert Doublet Model signatures at future e^+e^- colliders. *PoS*, EPS-HEP2019:570, 2020, 1911.06254.
- [44] Aleksander Filip Zarnecki, Jan Kalinowski, Jan Klamka, Pawel Sopicki, Wojciech Kotlarski, Tania Robens, and Dorota Sokolowska. Searching Inert Scalars

- at Future e^+e^- Colliders. In *International Workshop on Future Linear Colliders (LCWS 2019) Sendai, Miyagi, Japan, October 28-November 1, 2019*, 2020, 2002.11716.
- [45] Aleksander Filip Zarnecki, Jan Kalinowski, Jan Klamka, Pawel Sopicki, Wojciech Kotlarski, Tania Natalie Robens, and Dorota Sokolowska. Searching inert scalars at future e^+e^- colliders. *PoS*, CORFU2019:047, 2020.
 - [46] Jan Franciszek Klamka. Searching for Inert Doublet Model scalars at high energy CLIC. CERN-THESIS-2020-098, 2020.
 - [47] Expected performance of the ATLAS detector at the High-Luminosity LHC. Technical Report ATL-PHYS-PUB-2019-005, CERN, Geneva, Jan 2019.
 - [48] The CMS Collaboration. Expected performance of the physics objects with the upgraded CMS detector at the HL-LHC. Technical Report CMS-NOTE-2018-006. CERN-CMS-NOTE-2018-006, CERN, Geneva, Dec 2018.
 - [49] A. Abada et al. HE-LHC: The High-Energy Large Hadron Collider. *Eur. Phys. J. ST*, 228(5):1109–1382, 2019.
 - [50] A. Abada et al. FCC-hh: The Hadron Collider. *Eur. Phys. J. ST*, 228(4):755–1107, 2019.
 - [51] Jean Pierre Delahaye, Marcella Diemoz, Ken Long, Bruno Mansoulié, Nadia Pastrone, Lenny Rivkin, Daniel Schulte, Alexander Skrinsky, and Andrea Wulzer. Muon Colliders. 2019, 1901.06150.
 - [52] Tania Robens, Tim Stefaniak, and Jonas Wittbrodt. Two-real-scalar-singlet extension of the SM: LHC phenomenology and benchmark scenarios. *Eur. Phys. J.*, C80(2):151, 2020, 1908.08554.
 - [53] Andreas Papaefstathiou, Tania Robens, and Gilberto Tetlalmatzi-Xolocotzi. Triple Higgs Boson Production at the Large Hadron Collider with Two Real Singlet Scalars. 2020, 2101.00037.
 - [54] Rita Coimbra, Marco O. P. Sampaio, and Rui Santos. ScannerS: Constraining the phase diagram of a complex scalar singlet at the LHC. *Eur. Phys. J.*, C73:2428, 2013, 1301.2599.
 - [55] Raul Costa, Margarete Muehleitner, Marco O. P. Sampaio, and Rui Santos. Singlet Extensions of the Standard Model at LHC Run 2: Benchmarks and Comparison with the NMSSM. *JHEP*, 06:034, 2016, 1512.05355.
 - [56] Margarete Muehleitner, Marco O. P. Sampaio, Rui Santos, and Jonas Wittbrodt. ScannerS: Parameter Scans in Extended Scalar Sectors. 2020, 2007.02985.
 - [57] J R Andersen et al. Handbook of LHC Higgs Cross Sections: 3. Higgs Properties. 2013, 1307.1347.
 - [58] J. Alwall, R. Frederix, S. Frixione, V. Hirschi, F. Maltoni, O. Mattelaer, H. S. Shao, T. Stelzer, P. Torrielli, and M. Zaro. The automated computation of tree-level and next-to-leading order differential cross sections, and their matching to parton shower simulations. *JHEP*, 07:079, 2014, 1405.0301.
 - [59] Valentin Hirschi and Olivier Mattelaer. Automated event generation for loop-induced processes. *JHEP*, 10:146, 2015, 1507.00020.

- [60] M. Bahr et al. Herwig++ Physics and Manual. *Eur. Phys. J.*, C58:639–707, 2008, 0803.0883.
- [61] S. Gieseke et al. Herwig++ 2.5 Release Note. 2011, 1102.1672.
- [62] K. Arnold et al. Herwig++ 2.6 Release Note. 2012, 1205.4902.
- [63] J. Bellm et al. Herwig++ 2.7 Release Note. 2013, 1310.6877.
- [64] Johannes Bellm et al. Herwig 7.0/Herwig++ 3.0 release note. *Eur. Phys. J.*, C76(4):196, 2016, 1512.01178.
- [65] Johannes Bellm et al. Herwig 7.1 Release Note. 2017, 1705.06919.
- [66] Johannes Bellm et al. Herwig 7.2 release note. *Eur. Phys. J. C*, 80(5):452, 2020, 1912.06509.
- [67] M. Aaboud et al. Search for heavy ZZ resonances in the $\ell^+\ell^-\ell^+\ell^-$ and $\ell^+\ell^-\nu\bar{\nu}$ final states using proton–proton collisions at $\sqrt{s} = 13$ TeV with the ATLAS detector. *Eur. Phys. J.*, C78(4):293, 2018, 1712.06386.
- [68] Albert M Sirunyan et al. Search for a new scalar resonance decaying to a pair of Z bosons in proton-proton collisions at $\sqrt{s} = 13$ TeV. *JHEP*, 06:127, 2018, 1804.01939. [Erratum: JHEP03,128(2019)].
- [69] Morad Aaboud et al. Combination of searches for heavy resonances decaying into bosonic and leptonic final states using 36 fb^{-1} of proton-proton collision data at $\sqrt{s} = 13$ TeV with the ATLAS detector. *Phys. Rev.*, D98(5):052008, 2018, 1808.02380.
- [70] Albert M Sirunyan et al. Combination of searches for Higgs boson pair production in proton-proton collisions at $\sqrt{s} = 13$ TeV. *Phys. Rev. Lett.*, 122(12):121803, 2019, 1811.09689.
- [71] Georges Aad et al. Combination of searches for Higgs boson pairs in pp collisions at $\sqrt{s} = 13$ TeV with the ATLAS detector. *Phys. Lett.*, B800:135103, 2020, 1906.02025.
- [72] M. Cepeda et al. Report from Working Group 2. *CERN Yellow Rep. Monogr.*, 7:221–584, 2019, 1902.00134.
- [73] Morad Aaboud et al. Search for heavy resonances decaying into WW in the $e\nu\mu\nu$ final state in pp collisions at $\sqrt{s} = 13$ TeV with the ATLAS detector. *Eur. Phys. J.*, C78(1):24, 2018, 1710.01123.
- [74] HL-LHC prospects for diboson resonance searches and electroweak vector boson scattering in the $WW/WZ \rightarrow \ell\nu qq$ final state. Technical Report ATL-PHYS-PUB-2018-022, CERN, Geneva, Oct 2018.
- [75] Andreas Papaefstathiou and Graham White. The Electro-Weak Phase Transition at Colliders: Confronting Theoretical Uncertainties and Complementary Channels. 10 2020, 2010.00597.